

CO₂ condensation is a serious limit to the deglaciation of Earth-like planets

Martin Turbet

(martin.turbet@lmd.jussieu.fr)¹, Francois Forget¹, Jeremy
Leconte², Benjamin Charnay³, and Gabriel Tobie⁴

¹Laboratoire de Météorologie Dynamique, Sorbonne Universités,
UPMC Univ Paris 06, CNRS, 4 place Jussieu, 75005 Paris, France.

²Laboratoire d'astrophysique de Bordeaux, Univ. Bordeaux,
CNRS, B18N, allée Geoffroy Saint-Hilaire, 33615 Pessac, France.

³LESIA, Observatoire de Paris, PSL Research University, CNRS,
Sorbonne Universités, UPMC Univ. Paris 06, Univ. Paris Diderot,
Sorbonne Paris Cité.

⁴Laboratoire de Planétologie et Géodynamique, UMR-CNRS 6112,
University of Nantes, 2 rue de la Houssinière, F-44322 Nantes,
France.

September 29, 2018

Abstract

It is widely believed that the carbonate–silicate cycle is the main
agent, through volcanism, to trigger deglaciations by CO₂ greenhouse

warming on Earth and on Earth-like planets when they get in a frozen state. Here we use a 3D Global Climate Model to simulate the ability of planets initially completely frozen to escape from glaciation episodes by accumulating enough gaseous CO₂. The model includes CO₂ condensation and sublimation processes and the water cycle. We find that planets with Earth-like characteristics (size, mass, obliquity, rotation rate, etc.) orbiting a Sun-like star may never be able to escape from a glaciation era, if their orbital distance is greater than ~ 1.27 Astronomical Units (Flux $< 847 \text{ W m}^{-2}$ or 62% of the Solar constant), because CO₂ would condense at the poles – here the cold traps – forming permanent CO₂ ice caps. This limits the amount of CO₂ in the atmosphere and thus its greenhouse effect. Furthermore, our results indicate that for (1) high rotation rates ($P_{\text{rot}} < 24 \text{ h}$), (2) low obliquity (obliquity $< 23.5^\circ$), (3) low background gas partial pressures ($< 1\text{bar}$), and (4) high water ice albedo ($\text{H}_2\text{O albedo} > 0.6$), this critical limit could occur at a significantly lower equivalent distance (or higher insolation). For each possible configuration, we show that the amount of CO₂ that can be trapped in the polar caps depends on the efficiency of CO₂ ice to flow laterally as well as its gravitational stability relative to subsurface water ice. We find that a frozen Earth-like planet located at 1.30 AU of a Sun-like star could store as much as 1.5, 4.5 and 15 bars of dry ice at the poles, for internal heat fluxes of 100, 30 and 10 mW m⁻², respectively. But these amounts are in fact lower limits. For planets with a significant water ice cover, we show that CO₂ ice deposits should be gravitationally unstable. They get buried beneath the water ice cover in geologically short timescales of $\sim 10^4$ yrs, mainly controlled by the viscosity of water ice. CO₂ would be permanently sequestered underneath the water ice cover, in the form of CO₂ liquids, CO₂ clathrate hydrates and/or dissolved in subglacial water reservoirs (if any). This would considerably increase the amount of CO₂ trapped and further reduce the probability of deglaciation.

1 Introduction

There are geological evidences that Earth had to face multiple episodes of global or quasi-global glaciation, at the end of the Archean 2.45-2.22 Gya and during the Neoproterozoic era, 710 and 650 Mya (Evans et al., 1997; Hoffman et al., 1998; Hoffman and Schrag, 2002).

It is widely believed that the carbonate–silicate cycle (Walker et al., 1981; Kasting et al., 1993; Kump et al., 2000) was the main agent to trigger deglaciations on ancient Earth. In particular, on a completely frozen planet, also called ‘Hard Snowball’, the weathering of CO₂ is stopped ; continuous volcanic outgassing builds up atmospheric CO₂ that warm up the climate until liquid water is produced in the equatorial regions.

By extension, this mechanism may be crucial to stabilize the climate of Earth-like exoplanets. It is even central for the definition of the classical Habitable Zone (Kasting et al., 1993; Forget and Pierrehumbert, 1997; Kopparapu et al., 2013), which assumes that planets can build up CO₂ atmospheres (as massive as wanted) suitable for the stability of surface liquid water.

Planets near the outer edge of the Habitable Zone may suffer, as Earth did, episodes of complete glaciation. Recent work by Menou (2015) has even shown that, in the case of planets lacking land vascular plants, temperate climates may not be stable, because at high CO₂ partial pressure, the increased weathering rate does not allow temperate stable solutions. This effect, which is enhanced for planets weakly irradiated by their star, may systematically drive Earth-like exoplanets toward episodes of glaciation.

Can Earth-like planets in the Habitable Zone of their star always escape from episodes of glaciation ? In this work, we use 3D Global Climate Model (GCM) simulations of snowball planets to study the ability of the increased CO₂ greenhouse effect resulting from volcanic outgassing to drive them out of glaciation.

As the CO_2 outgassed by volcanoes accumulates in the atmosphere, the temperature of condensation of CO_2 can exceed the surface temperature of the poles. This leads to the trapping of extra outgassed CO_2 , forming permanent CO_2 polar ice caps, and thus seriously limits the efficiency of the carbonate–silicate cycle. This possibility has already been suggested in [Pierrehumbert \(2005\)](#) and [Pierrehumbert et al. \(2011\)](#), but has never been explored yet. We propose in this paper a detailed study of this scenario.

2 Method

We use in this paper the 3-Dimensions LMD Generic Global Climate Model to study the deglaciation of Earth-like planets orbiting in a circular orbit around a Sun-like star (Sun spectrum and luminosity) in response to increasing amounts of atmospheric CO_2 (from 0.01 to 3 bars), and for orbital distances ranging from 1.10 to 1.45 Astronomical Units (AU). Detailed information on the model can be found in [Appendix A](#).

Our simulations were designed to represent completely frozen Earth-like planet characteristics. These include the radius (6370 km), the gravity field (9.81 m s^{-2}), the obliquity (23.5°) and the rotation speed ($7.28 \times 10^{-5} \text{ rad s}^{-1}$). The roles of obliquity, planetary mass and rotation rate on the ability of planets to escape glaciation episodes are discussed in [sections 3.2 and 3.4](#). Eventually, most of the simulations were performed for a uniformly flat topography. The effect of topography is discussed in [section 3.4.5](#).

All the simulations performed in this study were forced initially in a cold and dry state, assuming:

1. A uniform and complete ice cover.
2. Atmospheric and surface temperatures arbitrarily fixed to 230 Kelvins

Explored parameters	Values
CO ₂ partial pressures (in bar)	[0.01, 0.1, 0.4, 1.0, 1.5, 2.0, 3.0]
i) Stellar flux (in W m ⁻²)	[1130, 1033, 949, 874, 808, 750, 697, 650]
ii) Flux compared to Earth (S _{eff})	[0.827, 0.756, 0.695, 0.640, 0.592, 0.549, 0.510, 0.476]
iii) Equivalent distance (in AU)	[1.10, 1.15, 1.20, 1.25, 1.30, 1.35, 1.40, 1.45]
Obliquity	0, 23.5°
CO ₂ ice clouds	radiatively active, inactive

Table 1: Physical Parameterizations used for GCM calculations.

everywhere.

3. No water vapor, no clouds.

Depending on CO₂ partial pressure, obliquity, or parameterization of clouds, the simulations evolve in different steady state climate regimes that are discussed in the next section.

3 Glaciation escape limited by CO₂ atmospheric collapse

3.1 Reference case

We performed 40 simulations of Earth-like planets (as described in section 2 – with a 23.5° obliquity and radiatively inactive CO₂ ice clouds) starting from an initially cold ($T = 230$ K everywhere) and global glaciation state for multiple irradiation fluxes and CO₂ partial pressures (see table 1). We fix the N₂ partial pressure to be constant and equal to 1 bar, in order to be consistent with the

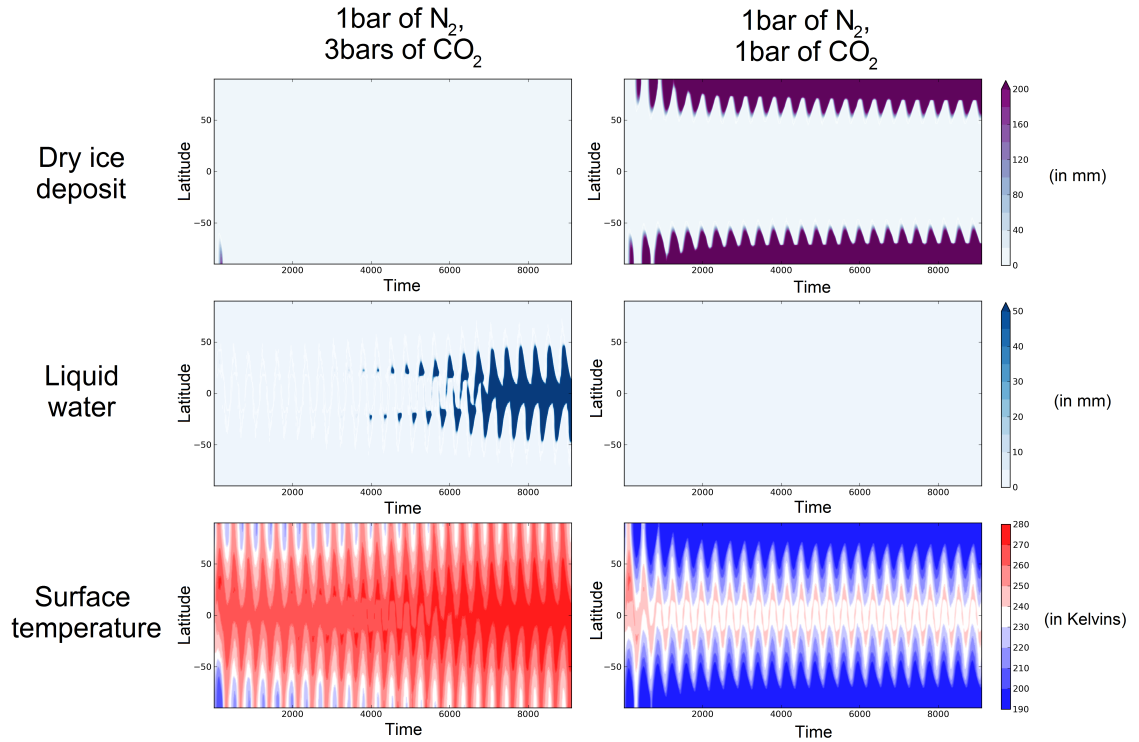


Figure 1: From top to bottom: Zonal means of (1) CO₂ ice deposit, (2) surface liquid water and (3) surface temperatures as a function of time (in Earth days), and for two different initial states. On left, the initially cold and dry planet starts with a CO₂ partial pressure of 3 bars and is able to escape glaciation. On right, the planet starts with a CO₂ partial pressure of 1 bar and ends up in atmospheric collapse. These simulations were run for planets with a 23.5° obliquity, radiatively inactive CO₂ ice clouds, and located at an equivalent orbital distance of 1.30 AU ($F = 808 \text{ W m}^{-2}$).

case of Earth. All simulations were run long enough to reach equilibrium¹.

We find that, depending on the CO₂ partial pressure and the stellar flux, these simulations can evolve in three different climate regimes:

1. The greenhouse effect of CO₂² is sufficient to raise the surface temperatures in equatorial regions above the melting temperature of water ice³. In this case, the positive feedback due to the decrease of the surface albedo (from 0.6 to 0.07) and the greenhouse effect of water vapor drive the planet out of glaciation.
2. The greenhouse effect of CO₂ is too weak to trigger a deglaciation. The planet stays in a snowball state.
3. The greenhouse effect of CO₂ is too weak to raise the surface temperatures of the poles above the condensation temperature of CO₂. In this case, atmospheric CO₂ collapses and the planet is locked in a global glaciated state, with two permanent CO₂ ice polar caps.

Figure 1 shows that, for a given solar flux (808 W m⁻² here), the choice of the initial CO₂ partial pressure can either drive the planet out of glaciation (pCO₂ = 3 bars) or cause a permanent collapse of the atmosphere at the poles (pCO₂ = 1 bar).

These results are summarized in Figure 2b, for multiple stellar fluxes and CO₂ partial pressures. Each region of the diagram denotes a steady state climate regime reached by the planet:

1. In red, the planet is partially or totally deglaciated.
2. In white, the planet is entirely frozen.

¹up to 30 Earth years for the thickest atmospheric configurations.

²which is enhanced by the pressure broadening of N₂.

³273 K, here.

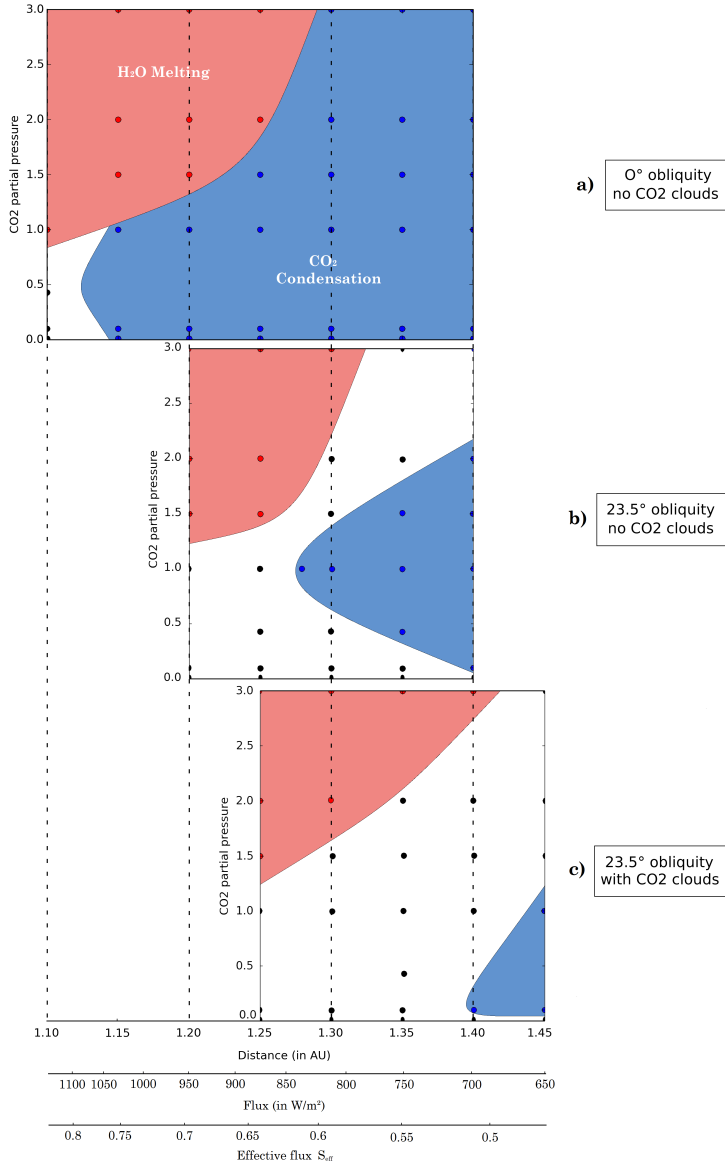


Figure 2: Climate regimes reached as function of the equivalent orbital distance from a Sun-like star (in AU) and the CO₂ partial pressure, assuming a cold start (i.e. snowball state without permanent CO₂ ice deposits). Diagrams a, b and c were constructed for Earth-like planets with 0° obliquity, 23.5° obliquity (reference simulation) and 23.5° obliquity with radiatively active CO₂ ice clouds, respectively. The red color roughly depicts the region where deglaciation is observed. The blue region represents glaciated states where CO₂ collapses permanently. The white region describes cases where none of this two previous conditions were reached.

3. In blue, the planet is entirely frozen and gaseous CO₂ has permanently collapsed at the poles. This situation actually occurs when winter CO₂ frost formation rate exceeds seasonal summer sublimation.

We now put these results in context of an active carbonate-silicate cycle. A planet that enters in a global glaciation state must have initially a low CO₂ atmospheric content that places it in the lower part of the diagram (in Figure 2b). From this point, CO₂ is outgassed by volcanoes and accumulates in the atmosphere. As the CO₂ partial pressure increases, the planet moves up in the diagram until:

1. the planet reaches the red zone first. The planet is able to escape glaciation.
2. the planet reaches the blue zone first. All the extra CO₂ possibly outgassed by volcanoes condenses at the poles and the planet is locked in a perpetual glaciation state.

For an (Earth-like) 23.5° obliquity, we find this limit to occur for planets located at more than 1.27 AU from a Sun-like star (Flux < 847 W m⁻², S_{eff}⁴ < 0.62), with an optimal CO₂ partial pressure around 1 bar (see Figure 2b).

However, if a planet starts with a large enough CO₂ atmospheric content so that it lies above the blue zone, then the CO₂ should resist atmospheric collapse and the deglaciation becomes possible.

3.2 Null obliquity case

For a 0° obliquity planet, because insolation in the polar regions is lowered, the equator-to-pole temperature contrast is amplified. Consequently, we find that

⁴The effective flux S_{eff} is defined as the ratio between the incoming stellar flux on the planet and that on the Earth.

permanent condensation of CO₂ at the poles happens for much lower equivalent distances ($d > 1.13$ AU, Flux < 1070 W m⁻², S_{eff} < 0.78 ; see Figure 2a).

3.3 Effect of CO₂ ice clouds

During polar nights, the temperatures at the poles are very low. CO₂ condenses at the surface but also in the atmosphere, forming CO₂ ice clouds that may have a significant warming effect (Forget and Pierrehumbert, 1997).

We performed multiple simulations for planets at 23.5° obliquity including radiatively active CO₂ ice clouds. For this, we used a constant cloud condensation nuclei [CCN] of 10⁵ kg⁻¹ designed to maximize the greenhouse effect of CO₂ ice clouds (Forget et al., 2013). This idealized configuration corresponds to an endmember description of the radiative warming effect of CO₂ ice clouds. In particular, Kitzmann (2016) has shown recently, using a more refined radiative transfer scheme, that a configuration like the one used in this section probably overestimates the warming effect of CO₂ ice clouds.

Our simulations (example in Figure 3.3) show that the CO₂ ice clouds distribution evolves significantly with seasons. In winter, CO₂ ice clouds form a quasi-complete polar cover and have a powerful greenhouse effect that limits the condensation of CO₂ at the poles. In summer, CO₂ clouds dissipate as insolation increases. As a result, CO₂ clouds have a very limited impact on the albedo and therefore do not contribute much to prevent polar CO₂ ice summer sublimation.

For these two reasons, CO₂ ice clouds seriously limit the collapse of CO₂ at the poles. Figure 2c shows that, with radiatively active CO₂ clouds, CO₂ condensation would occur for equivalent distance > 1.40 AU (Flux < 697 W m⁻², S_{eff} < 0.51).

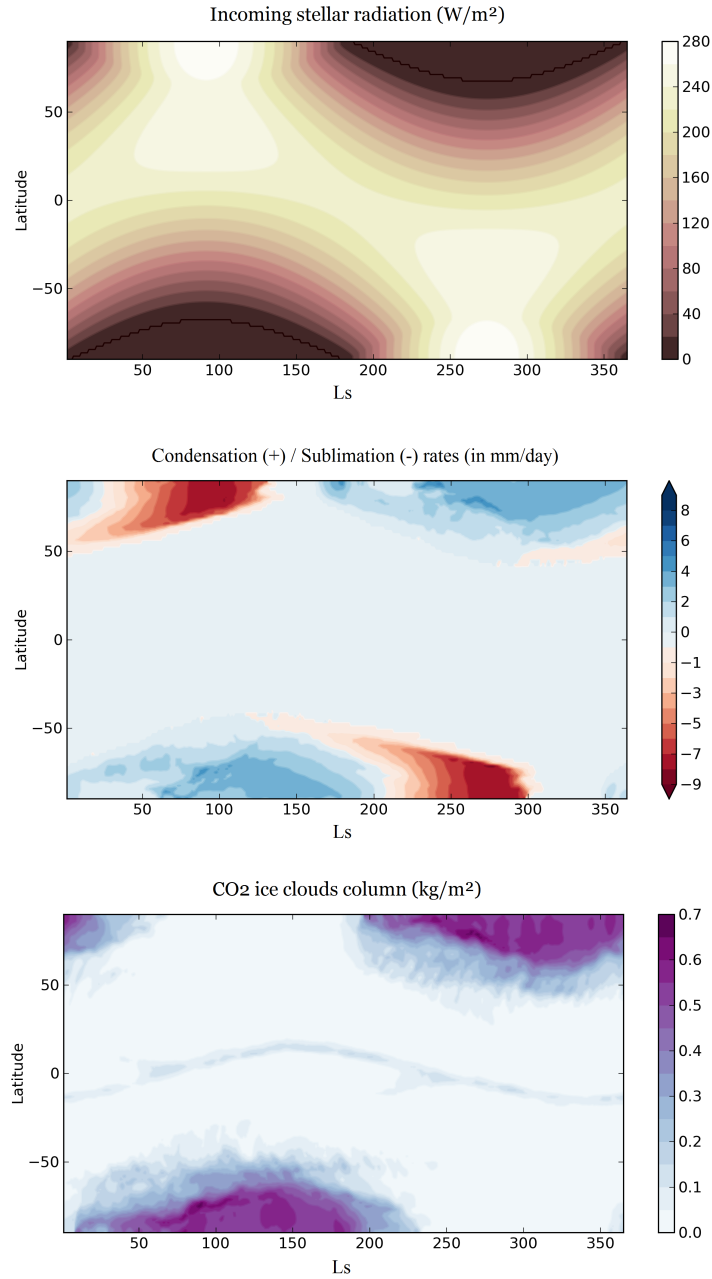


Figure 3: From top to bottom: (1) zonal mean of incoming stellar radiation (ISR) versus L_s , (2) zonal mean of CO_2 ice condensation(+)/sublimation(-) rates versus L_s , and (3) zonal mean of CO_2 ice cloud (column integrated) content versus L_s . These figures were computed for a planet with a 23.5° obliquity, active CO_2 ice clouds, located at an equivalent orbital distance of 1.40 AU ($F = 697 \text{ W m}^{-2}$) and for a CO_2 partial pressure of 1 bar and a N_2 partial pressure of 1 bar.

3.4 Sensitivity study

3.4.1 The albedo of ices

The choice of water ice albedo can severely affect our results. For albedo higher than 0.67, we find that CO₂ condensation can occur on Earth-like planets (23.5° obliquity, radiatively inactive CO₂ ice clouds) for equivalent distance as low as 1.15 AU (Flux $\sim 1033 \text{ W m}^{-2}$, $S_{\text{eff}} \sim 0.76$), corresponding to the reduced luminosity of the Sun 3.8 Gya calculated from standard solar evolution models (Gough, 1981).

We note that water ice albedo is considerably reduced around cool stars (Joshi and Haberle, 2012), making the scenario of CO₂ polar condensation less efficient. However, planets orbiting in the Habitable Zone of M-dwarfs are also subject to tidal locking. The temperature on the nightside of a synchronous planet can be extremely low, favoring the CO₂ condensation. This possibility is explored and discussed in details in Turbet et al. 2017b.

We also explored the effect of CO₂ ice albedo that could potentially be very high (see section A.3, Kieffer et al. 2000) and we found it to be much less important.

Eventually, we acknowledge that a real Snowball might have regions of open continent not covered by water ice, which would lower albedo. These could act as sources of dust, and volcanic aerosols could also darken the surface (Abbot and Pierrehumbert, 2010).

3.4.2 The rotation rate

The rotation rate of Earth has evolved in time from 1.2×10^{-4} (4 Gya) to $7.3 \times 10^{-5} \text{ rad s}^{-1}$ (now) due to the effect of the Moon's tidal friction (Walker and Zahnle, 1986; Zahnle and Walker, 1987). More generally, Earth-like planets could harbor a wide range of rotation rates.

In this study, we find that rotation rate is a very important parameter for CO₂ polar condensation. A high rotation rate reduces the latitudinal transport and thus increases the equator-to-pole surface temperature gradient (Kaspi and Showman, 2015), favoring CO₂ condensation at the poles. We find that, for a rotation rate $\Omega = 4 \Omega_{\text{Earth}}$ (23.5° obliquity, radiatively inactive CO₂ ice clouds), CO₂ can collapse as early as 1.15 AU (Flux $\sim 1033 \text{ W m}^{-2}$, $S_{\text{eff}} \sim 0.76$).

To go further, we investigated the case of Archean Earth, 3.8 Gya ($S_{\text{eff}} \sim 0.76$), through simulations of a completely frozen planet, assuming a 23.5° obliquity, a rotation period of 14 hours and a water ice albedo set to 0.6. We find that CO₂ can condense at the poles seasonally, but never permanently.

3.4.3 The planetary mass

Massive planets also have a large radius that may be responsible for the weakening of the poleward heat transport, favoring the collapse of CO₂. For example, assuming an internal composition similar to the Earth, a 5 M_{Earth} planet would have a radius around 1.5 R_{Earth} or 10^4 km (Seager et al., 2007). We performed GCM simulations for a 5 M_{Earth} planet, for a CO₂ partial pressure of 1 bar and a N₂ partial pressure of 1 bar. In these conditions, we find that the collapse of CO₂ can occur for equivalent distances as low as 1.18 AU (Flux $< 981 \text{ W m}^{-2}$, $S_{\text{eff}} < 0.72$).

However, because accretion of volatiles should increase with planetary mass, the atmospheric mass should also increase with it (see Kopparapu et al. (2014) section 2 for more details). Therefore, we expect a massive planet to have a greater content of background gas (e.g. N₂). For a 5 M_{Earth} planet, assuming that P_{surface} scales as $R_{\text{planet}}^{2.4}$. (equation 3 in Kopparapu et al. (2014)), we roughly get a partial pressure of N₂ equal to 3.3 bars⁵. Using GCM simulations,

⁵We remind the reader that volatile delivery to a planet is stochastic in nature and may be a weak function of planetary mass. By way of comparison, Venus (at $\sim 0.8 M_{\text{Earth}}$) has ~ 3 bars of N₂ in its atmosphere.

we find that in this more realistic case, CO₂ collapses for equivalent distances greater than 1.30 AU (Flux < 808 W m⁻², S_{eff} < 0.59).

3.4.4 The atmospheric composition: the role of N₂ partial pressure

The result of the previous section shows that N₂ partial pressure can have a significant impact on CO₂ collapse. As pN₂ increases, the atmosphere thickens and (1) the poleward heat transport increases and (2) the greenhouse effect of CO₂ increases because of pressure broadening of CO₂ by N₂. Both effects tend to prevent CO₂ condensation.

Quantitatively, our simulations show that, for an Earth-like planet with a CO₂ partial pressure of 1 bar (with 23.5° obliquity, radiatively inactive CO₂ ice clouds), doubling pN₂ from 1 to 2 bars leads to the condensation of CO₂ for equivalent orbital distances greater or equal to 1.35 AU (+0.08 AU difference).

3.4.5 The topography

To investigate the possible effects of topography on CO₂ polar condensation, we ran several simulations in which we emplaced a mountain range similar in size to the Himalaya (5000 km altitude plateau, 10⁶ km²) at several latitudes (0°N, 30°N, 45°N, 60°N, 90°N). We find that CO₂ permanent condensation can occur on top of the mountain range for distances lower than 1.27 AU, only for latitudes greater than 45°N. For the 60°N latitude case, CO₂ condensation starts as low as 1.20 AU (Flux ~ 949 W m⁻², S_{eff} ~ 0.69).

Nonetheless, the total amount of CO₂ that could condense and be trapped above a mountain range is rather low, because it is limited by the area of the mountain range.

4 How much CO₂ ice can be trapped ?

In this section, we investigate two processes that should control the amount of CO₂ that can be trapped on the surface or subsurface: 1) flows of polar CO₂ ice to lower latitudes and sublimation; and 2) burial of CO₂ ice beneath the water ice cover due to higher density.

4.1 Maximum size of CO₂ ice glaciers

At first sight, the main limit of the trapping of CO₂ as ice instead of greenhouse gas is the size of the solid CO₂ polar reservoirs. When CO₂ is outgassed by volcanoes, the atmospheric pressure stays constant but the size of the CO₂ polar caps grows. At some point, the CO₂ ice caps form glaciers that can flow efficiently toward equatorial regions, CO₂ ice being much less viscous than water ice. In the process, CO₂ ice can be sublimated and reinjected in the atmosphere.

In this section, we give estimates of the maximum amount of CO₂ that can be trapped in steady state CO₂ ice polar caps, for a planet with a 23.5° obliquity, radiatively inactive CO₂ ice clouds, located at a distance of 1.30 AU ($F = 808 \text{ W m}^{-2}$) and for both CO₂ and N₂ partial pressures set to 1 bar.

4.1.1 CO₂ ice caps radial extent

First, we get from our GCM simulations the radial extent of the two permanent CO₂ ice polar caps, defined for a positive annual mean CO₂ condensation rate. We note the corresponding radius of the ice cap $R_{\text{cap},1}$. Then, in GCM simulations, we artificially extend (in the radial direction) the CO₂ ice caps to take into account the glacier flow, until the net globally averaged annual condensation/sublimation rate vanishes. In practice, we used the following algorithm:

1. We run the simulation until globally averaged annual mean rate of condensation/sublimation is constant.
2. If this rate is (roughly) null, CO₂ ice caps are in a dynamical equilibrium. We stop here.
3. If this rate is positive, we artificially increase the size of the CO₂ ice caps of one GCM grid (in the latitudinal direction, and for each longitude) by emplacing arbitrarily a large enough amount of CO₂ ice. We go back to step 1.

This method gives us a good estimate of the steady state maximal extent of the CO₂ ice polar caps. We note the corresponding radius of the ice cap $R_{\text{cap},2}$. With and without glacier flow, we obtain polar cap radii $R_{\text{cap},1} = 2070$ km and $R_{\text{cap},2} = 2800$ km. This corresponds to a latitudinal extent down to 71.5°N and 65°N ⁶, respectively. Figure 4 shows zonal condensation/sublimation annual mean rates along the North Pole CO₂ glacier.

In total, the two CO₂ ice caps have an area of 27 millions of km² (respectively 49 millions of km² if considering the glacier flow). This corresponds to 5% (respectively 10%) of the total area of the (Earth-like) planet.

4.1.2 CO₂ ice cap inner region: a thickness limited by basal melting

In the region within the CO₂ ice caps with positive annual mean condensation rates, the CO₂ ice maximum thickness should be mainly limited by basal melting induced by the geothermal heat flux, noted F_{geo} .

Assuming that the temperature inside the CO₂ glacier rises linearly with depth, with a lapse rate fixed by the geothermal heat flux (conductive regime),

⁶By symmetry, results are identical in the southern hemisphere.

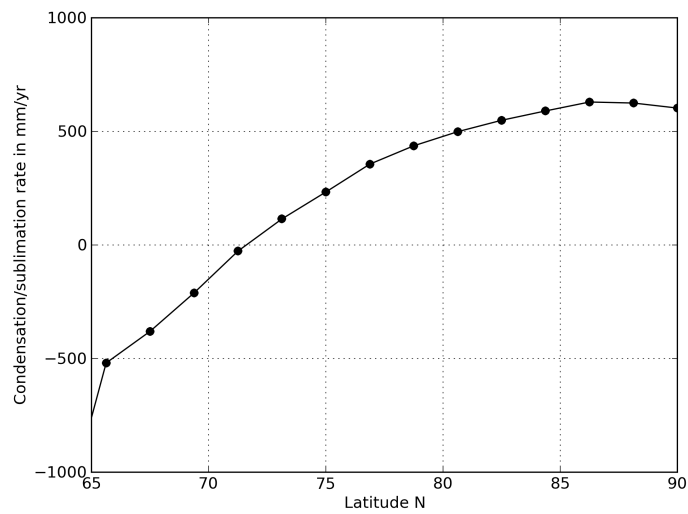


Figure 4: Zonal and annual mean CO_2 condensation/sublimation rates along the CO_2 northern ice cap, for the reference case (1.30 AU equivalent distance, 23.5° obliquity and radiatively inactive CO_2 ice clouds). It corresponds also to the $a(r)$ function (see section 4.1.3). Positive values correspond to latitudes where the annual mean CO_2 condensation rate is positive. These are locations where CO_2 condenses permanently. Negative values are "potential" sublimation rates, i.e. it is assumed that CO_2 ice is available – following the algorithm described in section 4.1.1 – and can sublime all year long.

the maximum CO₂ ice thickness h_{\max} is given by:

$$h_{\max} = \frac{\lambda_{\text{CO}_2} (T_{\text{melt}} - T_{\text{surf}})}{F_{\text{geo}}}, \quad (1)$$

where λ_{CO_2} is the thermal conductivity of CO₂ ice, T_{surf} is the temperature at the top of the glacier and T_{melt} is the melting temperature of CO₂ ice at the base of the glacier. As the latter is a function of the pressure below the CO₂ glacier, it implicitly depends on h_{\max} so that the above equation must be solved numerically, once the local surface temperature is known (see Appendix B for details on the calculations). The resulting maximum CO₂ ice cap thickness h_{\max} is plotted on Figure 5 as a function of the internal heat flux and the CO₂ partial pressure. For geothermal heat fluxes of 100/30/10 mW m⁻² (red stars in Figure 5), basal melting condition gives CO₂ ice maximum thicknesses of 120/360/1200 m.

The exact latitude at which the glacier maximum thickness is determined by either basal melting condition or by glacier flow is difficult to determine. Moreover, in the region of transition between these two regimes, a basal liquid CO₂ flow could persist⁷ and therefore speed up the glacier flow.

For simplicity, we fixed the thickness of the steady-state CO₂ glacier in the regions with positive annual mean condensation rate (regions of latitude > 71.5°N ; see Figure 4) at the constant maximum thickness h_{\max} derived from the basal melting condition. This maximum thickness serves as a boundary condition for the calculation of the glacier flow in regions with positive annual mean sublimation rate (see next section).

⁷Such basal flow could carry heat away from basal melting regions and thus also reduce the heat flux conducted through the CO₂ ice caps (Cuffey and Paterson, 2010; Menou, 2013).

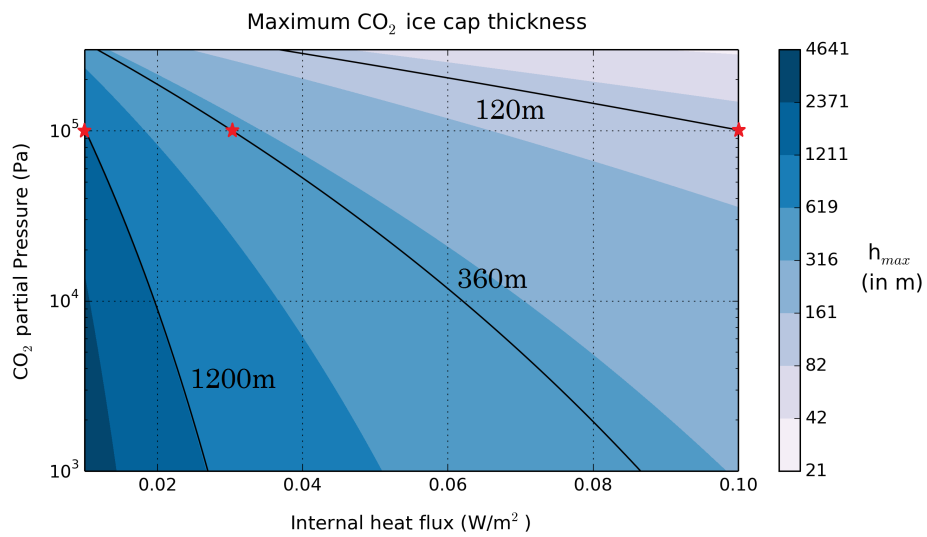


Figure 5: CO₂ ice cap maximum thickness (in m) calculated from the basal melting condition, as a function of surface CO₂ partial pressure and internal heat flux. The red stars correspond to three distinct cases, with pCO₂ = 1bar and $F_{\text{geo}} = 10 / 30 / 100 \text{ mW m}^{-2}$, that are investigated in more details in the following sections.

4.1.3 CO₂ ice cap outer region: a thickness limited by glacier flow and sublimation

To get estimates of CO₂ glacier profiles in the regions where sublimation dominates over condensation (latitude < 71.5°N, see Figure 4), we use a simple isothermal glacier model ⁸ (assuming no slip at the base of the glacier), following a similar approach than Menou (2013). The steady-state equation satisfied by a thin isothermal CO₂ glacier with a flat base and a no slip boundary condition at its bottom is (Fowler, 2011; Paterson, 2010)⁹:

$$\frac{1}{r} \frac{\partial}{\partial r} \left(r \frac{2A_0(\rho g)^n}{n+2} h^{n+2} \left| \frac{\partial h}{\partial r} \right|^{n-1} \frac{\partial h}{\partial r} \right) + a(r) = 0, \quad (2)$$

with $h(r)$ the thickness of the CO₂ ice cap, assumed (for simplicity) radially symmetric, A_0 the flow rate constant (in Pa s⁻ⁿ), n the power-law creep exponent, g the surface gravity, ρ the density of CO₂ ice and $a(r)$ the annual mean condensation rate assumed (also for simplicity) to be a function of r only, and derived from our GCM simulations (see Figure 4).

First, assuming $\frac{\partial h}{\partial r} = 0$ for $r = R_{\text{cap},1}$, we integrate equation 2 once. Then, assuming $h > 0$, $\frac{\partial h}{\partial r} < 0$ and $a(r) < 0$, we separate the variables h and r , and we integrate a second time, assuming $h(R_{\text{cap},2}) = 0$ at the edge of the glacier. Eventually, assuming that $h(R_{\text{cap},1}) = h_{\text{max}}$, with h_{max} the maximum thickness of the glacier calculated using the basal melting condition, we can constrain the flow rate A_0 and get the following solutions for the thickness h of the CO₂ ice glacier:

$$h(r) = h_{\text{max}} \text{ for } r \leq R_{\text{cap},1}, \quad (3)$$

⁸This is a simple approach that does not physically describe how the accumulating CO₂ ice spreads to feed the ablation zone. We acknowledge that a more physically complete model should be developed in the future.

⁹This is the classic solution for a glacier shape.

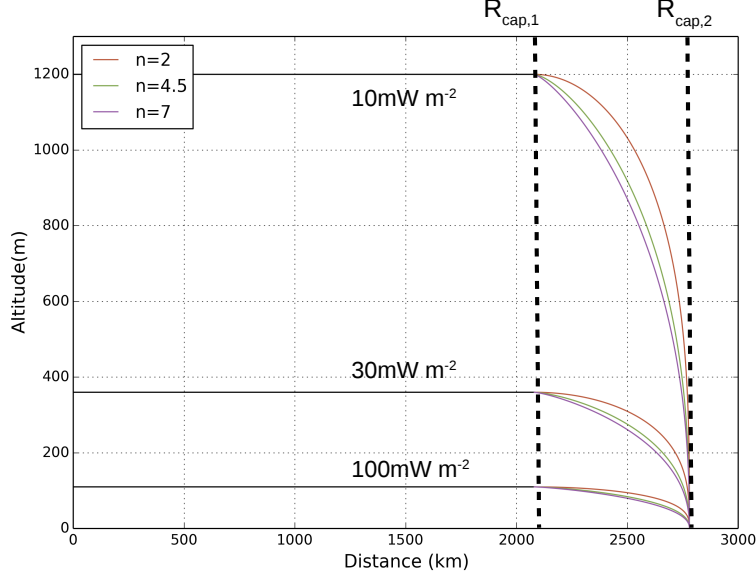


Figure 6: Possible radial profiles for the CO₂ ice polar glaciers. They correspond to solutions of equations 3 and 4, for 3 different internal heat fluxes (10/30/100 mW m⁻²) and three different flow laws (n = 1, 4.5 and 7).

$$h(r) = h_{\max} \left(\frac{\int_r^{R_{\text{cap},2}} \left(-\frac{1}{r_2} \int_{R_{\text{cap},1}}^{r_2} r_1 a(r_1) dr_1 \right)^{\frac{1}{n}} dr_2}{\int_{R_{\text{cap},1}}^{R_{\text{cap},2}} \left(-\frac{1}{r_2} \int_{R_{\text{cap},1}}^{r_2} r_1 a(r_1) dr_1 \right)^{\frac{1}{n}} dr_2} \right)^{\frac{n}{2n+2}} \quad \text{for } r > R_{\text{cap},1}, \quad (4)$$

Figure 6 presents 9 possible steady-state CO₂ ice glacier profiles, for 3 different geothermal fluxes and 3 different flow laws (n = 1, 4.5 and 7) chosen consistent with previous experimental studies (Durham et al., 1999) and works about the martian CO₂ southern polar cap (Nye et al., 2000).

4.1.4 Calculation of the CO₂ maximum total reservoir

After integration of the steady state CO₂ ice radial profiles, we find that the maximum amount of CO₂ ice that can be stored in the two polar caps is approximately equal to 1.5/4.5/15 bars¹⁰ for geothermal heat fluxes of 100/30/10 mW m⁻², respectively. On Earth, the current geothermal heat flux is ~ 80 mW m⁻² but can vary a lot, typically from 20 mW m⁻² up to 400 mW m⁻², depending on the regions (Davies, 2013). Approximately 60% (respectively 40%) of CO₂ ice is trapped in region of $r < R_{\text{cap},1}$ (respectively $r > R_{\text{cap},1}$), meaning that the accumulation zone and the ablation zone contribute significantly and equally to the total size of the CO₂ ice reservoir.

It is now possible to calculate, for a given rate of CO₂ volcanic outgassing, the time required for a hard snowball planet to fill the CO₂ ice polar reservoirs and thus potentially escape glaciation. Assuming a present-day Earth CO₂ volcanic outgassing rate of ~ 7 teramoles/year or 60 bars/Gy (Brantley and Koepnick, 1995; Jarrard, 2003), we get durations of glaciation periods of $\sim 42/93/270$ My for internal heat fluxes of 100/30/10 mW m⁻². In fact, because CO₂ volcanic outgassing rate is dependant on the internal heat flux, the duration of the glaciation phases could be drastically increased for planets with low geothermal heat fluxes (typically lower than 80 mW m⁻² as on present-day Earth). This suggests that planets near the outer edge of the habitable zone may need to be quite volcanically active in order to remain habitable.

When (and if) CO₂ ice caps become full, the system suddenly reaches a runaway phase, ending up with the complete vaporization of CO₂ polar ice caps and thus a hot atmosphere. This may have implications in the calculation and description of 'limit-cycles' (Menou, 2015; Haqq-Misra et al., 2016; Abbot, 2016) and more generally on the habitability of distant Earth-like planets. De-

¹⁰These quantities are not affected much by the choice of flow law (see Figure 6).

tailed calculations of the stability of CO₂ ice caps when full can be found in Appendix C.

It is also conceivable that catastrophic events such as meteoritic impacts could trigger deglaciation.

4.2 Gravitational stability and CO₂ sequestration

For planets covered by several hundred meters of water ice¹¹, owing to the high density of CO₂ ice ($\sim 1500 \text{ kg m}^{-3}$) or liquids ($\sim 1170 \text{ kg m}^{-3}$) compared to water ice ($\sim 930 \text{ kg m}^{-3}$ at 200-220 K), the CO₂ deposits should rapidly become gravitationally unstable. This would result in a burial of the CO₂ deposits at the base of the H₂O ice layer. Such a density contrast should initiate Rayleigh-Taylor instabilities at a timescale that can be estimated at first order assuming two isoviscous layers using the following relationship (Turcotte and Schubert, 2001):

$$\tau_{\text{RT}} = \frac{13 \eta}{\Delta \rho g b}, \quad (5)$$

with η the viscosity of the more viscous layer, $\Delta \rho$ the density contrast between the two layers and b the characteristic size of the domain. Depending whether CO₂ is liquid or solid at the interface with the H₂O layer, the density contrast would range between 240 and 570 kg m⁻³. For a CO₂ ice deposit thickness of about 100 m, this density contrast results in a stress at the interface between the two layers of the order of 1 MPa. For such a stress level and temperature ranging between 200 and 220 K, the viscosity of the CO₂ ice layer is estimated between 10¹²-10¹³ Pa s, based on available experimental data (Durham et al., 1999). At the same temperature and stress conditions, water ice has a viscosity $\leq 10^{16}$ Pa s, for grain size lower than 1 mm, based on experimental data (Durham et al.,

¹¹We remind here that the Earth Global Equivalent Layer of surface water is ~ 3 km.

2001; Durham and Stern, 2001; Goldsby and Kohlstedt, 2001). Therefore, this would be the layer controlling the Rayleigh-Taylor timescale. Assuming that a thickness of 100 m of CO₂ deposit is representative of the characteristics size of the domain, the R-T timescale is $7 \times 10^3 \text{ yrs} \times (\eta/10^{16} \text{ Pa s})$, which is geologically short. In the case of basal melting of the CO₂ layer, we should keep in mind that the generated CO₂ liquids will be unstable relative to the underneath water ice layer, but also relative to the overlying CO₂ ice layer as it has a density intermediate between those of CO₂ ice and water ice. When CO₂ melting occurs at the base of the CO₂ layers, a competition is expected between downward drainage through the water ice layer (similar to crevasse hydrofracturing in Earth's glaciers; Krawczynski et al. 2009) and liquid injection in the overlying CO₂ ice layer and refreezing (similar to dike propagation). Assessing in details such complex processes are out of scope of the present paper. Nevertheless, based on these considerations, we can safely argue that the accumulation of a large volume of liquid CO₂ at the base of the CO₂ ice layer is unlikely.

Once gravitationally destabilized, the CO₂ ice deposit would sink at the base of the water ice shell at a rate that is determined mostly by the viscosity of water ice and the size of the CO₂ ice diapir. The time required for a CO₂ ice diapir to cross the water ice layer can be estimated using the Stokes velocity, the terminal velocity of a sphere falling through a constant viscosity medium (Ziethe and Spohn, 2007):

$$U_s = \frac{2}{9} \Delta \rho g (r^2/\eta) \quad (6)$$

For a diapir radius r of 100 m (comparable to thickness of the CO₂ deposit) and a viscosity of water ice of 10^{15} - 10^{16} Pa s, this leads to a velocity of 0.04-0.4 m/yr. As temperature increases as a function of depth, the viscosity of water ice is

expected to decrease with depth, resulting in an acceleration of the diapir fall. A 100-m diapir of CO₂ ice would thus not need more than $\sim 10^4$ yrs to reach the bottom of a 1-km thick water ice layer.

Even if the CO₂-H₂O interface is beneath the melting temperature of CO₂ ice, melting may occur during the diapir fall, which will reduce the density contrast and hence the fall velocity. However, as mentioned above, melting may promote fracturing of the water ice medium and rapid drainage of the CO₂ liquids due to its high density relative to the surrounding water ice. The rate of melting should also depend on the efficiency of heat transfer between the diapir and the surrounding ice. As the thermal diffusive timescale ($\sim r^2/\kappa$) for a 100-m-size diapir of CO₂ is of the order of 10^3 yrs and is thus \leq to the expected diapir fall timescale, melting during the descent would be efficient. Detailed modelling would be required though to determine the exact volume of generated melt during descent.

CO₂ ice should completely melt and equilibrate thermally with the surrounding H₂O media once stabilized at the bottom of the water ice shell. The temperature and pressure conditions at the bottom of the water ice layer depend on its thickness and on the geothermal flow. For geothermal heat flux between 50 and 100 mW m^{-2} , typical of the Earth, the melting of water ice would be reached for depth ranging between 1.5 and 3 km, corresponding to pressure of about 14 and 28 MPa. This pressure range is well above the saturation vapor pressure (3.5 MPa at 273 K; [Lide 2004](#)), so that CO₂ is highly stable in the liquid phase. Destabilizing the CO₂ liquids into gas phase would require the 273 K-isotherm at a depth of only 375 m, corresponding to abnormally high geothermal heat flux of 400 mW m^{-2} , 5 times larger than the average heat flux on Earth. Even if the density of liquid CO₂ decreases with increasing temperature as it equilibrates with the surrounding water ice media, it remains always

denser than water ice (Span and Wagner, 1996), and therefore should always accumulate at the bottom of the ice shell. At $T = 273$ K and pressure between 14 and 28 MPa, CO_2 liquids have a density very close to that of liquid water (994 and 1048 kg m^{-3} , respectively, using the equation of state of Span and Wagner (1996)), so that CO_2 coexists with H_2O at the ice-water interface.

Pressure and temperature conditions expected at the bottom of the ice layer are in the stability field of CO_2 clathrate hydrate (Sloan, 1998; Longhi, 2005), therefore CO_2 should rapidly interact with H_2O molecules to form clathrate hydrate. Clathrate hydrates are non-stoichiometric compounds consisting of hydrogen-bonded H_2O molecules forming cage-like structures in which guest gas molecules, such as CO_2 , can be trapped (Sloan, 1998). Once formed, these clathrates are very stable and can be dissociated only if the temperature is raised about 5-10 K above the melting point of water ice. The storage of CO_2 in the form of clathrate should be particularly efficient in the case of warm bottom conditions as CO_2 liquids and liquid water coexist. In the cold bottom condition with no water ice melting, clathration is still possible but would be less efficient due to the physical separation between the two components. As CO_2 clathrate hydrate has a density of about 1150 kg m^{-3} (assuming full cage occupancy, Sloan (1998)), they would rapidly sink at the bottom of the water liquid layer, ensuring an almost complete clathration of CO_2 . Part of the CO_2 should dissolve in the liquid water during the clathrate sinking. The relative proportion of CO_2 trapped in the form of clathrate hydrate or dissolved in the water layer would depend on the volume of CO_2 that is buried at the base of the ice shell and on the volume (thickness) of the water layer.

In summary, as long as the water ice shell exceeds a few hundred meters, CO_2 should remain sequestered either in the form of CO_2 liquids, in the form of CO_2 clathrate hydrate or dissolved in the subglacial water layer. Release

of gaseous CO_2 may occur only due to an increase of surface insulation and increase of geothermal flux resulting in a significant thinning and breaking-up of the water ice shell. The total amount of CO_2 that can be stored in the H_2O layer (by any of these three processes) depends on the total abundance of H_2O of the planet as well as $\text{CO}_2/\text{H}_2\text{O}$ ratio. The CO_2 inventory on Earth, mostly in the form of carbonate rocks on the continents, is of the order of 10^2 bars (Walker, 1985). If the total CO_2 inventory exceeds the total amount of CO_2 that can be stored in the water layer, then the planet should be able at some point to escape from global glaciation, extra CO_2 being likely returned to the atmosphere through cryovolcanism.

Evaluating the maximum amount of CO_2 that can be trapped underneath the water ice cover require however a detailed description of the H_2O layer structure as well as thermodynamic models predicting the partitioning of CO_2 between the different phases.

5 Conclusions

We highlight in this paper a new scenario that would prevent distant Earth-like planets orbiting Sun-like stars from escaping episodes of complete glaciation. When a terrestrial planet reaches a Snowball state, CO_2 weathering ceases and CO_2 can accumulate in the atmosphere because of volcanic outgassing. As CO_2 builds up in the atmosphere, the temperature of condensation of CO_2 can exceed the surface temperature of the poles, which leads to the trapping of all extra CO_2 possibly outgassed.

Using LMD Global Climate Model simulations designed for Earth-like fully glaciated planets, we show that this mechanism can work from orbital distances as low as 1.27 AU (Flux $\sim 847 \text{ W m}^{-2}$, $S_{\text{eff}} \sim 0.62$). By comparison, the most recent estimate of the outer edge of the Habitable Zone (e.g. the maxi-

mum greenhouse limit) in similar conditions is 1.67 AU (Flux $\sim 490 \text{ W m}^{-2}$, $S_{\text{eff}} \sim 0.36$) (Kopparapu et al., 2013).

This limit can occur at even lower distances for planets with 1) a low obliquity, 2) a low N_2 partial pressure, 3) a high rotation rate and 4) a high value of the water ice albedo (we chose in this work the conservative value of 0.6).

Conversely, this limit can occur at significantly higher distances when taking into account the radiative effect of CO_2 ice clouds. In winter, CO_2 ice clouds that form at the cold poles scatter back thermal infrared radiation of the surface. In summer, clouds are dissipated and therefore have almost no impact on the bond albedo. For these two reasons, CO_2 ice clouds can have a powerful warming effect at the poles, limiting CO_2 collapse at orbital distances greater than 1.40 AU (Flux $< 697 \text{ W m}^{-2}$, $S_{\text{eff}} < 0.51$).

For each possible configuration, the amount of CO_2 that can be trapped in polar CO_2 ice caps depends on the efficiency of CO_2 ice to flow laterally as well as its gravitational stability relative to subsurface water ice. The flow of CO_2 ice from polar to low latitudes regions is mostly controlled by its basal temperature (due to both the conductivity and melting temperature of CO_2 ice being low), and hence by the internal heat flux of the planet. We find for example that a frozen Earth-like planet located at 1.30 AU of a Sun-like star could store as much as 1.5/4.5/15 bars of CO_2 ice at the poles, for internal heat fluxes of 100/30/10 mW m^{-2} .

But these amounts are in fact lower limits. CO_2 ice being denser than water ice ($\sim 1.7 \times$ the volumetric mass of water ice), we find that CO_2 ice deposits should be gravitationally unstable and get buried beneath the water ice cover in a geologically short timescale of $\sim 10^4$ yrs, mainly controlled by the viscosity of water ice. If water ice cover exceeds about 300 meters (e.g. 10% of the Earth hydrosphere), then CO_2 should be permanently sequestered underneath the water

ice cover, in the form of CO₂ liquids, CO₂ clathrate hydrates and/or dissolved in subglacial water reservoirs (if any). This would considerably increase the amount of CO₂ trapped and further reduce the probability of deglaciation.

6 acknowledgements

M.T. thanks Emmanuel Marcq for fruitful discussions related to this work during the legendary LMD PLANETO meetings. We acknowledge the feedbacks from Jim Kasting, William B. McKinnon, Dorian Abbot and an anonymous referee, which improved both the style and content of the manuscript. This project has received funding from the European Research Council (ERC) under the European Unions Horizon 2020 research and innovation programme (grant agreement No. 679030/WHIPLASH).

A The LMD Generic Global Climate Model

A.1 Model core

This model originally derives from the LMDz 3-dimensions Earth Global Climate Model (Hourdin et al., 2006), which solves the primitive equations of geophysical fluid dynamics using a finite difference dynamical core on an Arakawa C grid.

The same model has been used to study many different planetary atmospheres of low-irradiated planets, including Archean Earth (Charnay et al., 2013), past climates of Mars (Forget et al., 2013; Wordsworth et al., 2013; Turbet et al., 2017a), or exoplanets (Wordsworth et al., 2011; Turbet et al., 2016, 2017b).

The simulations presented in this paper were all performed at a horizontal resolution of 96×96 (e.g. $3.75^\circ \times 1.875^\circ$) in longitude \times latitude. In the

vertical direction, the model is composed of 15 distinct atmospheric layers that were designed using hybrid σ coordinates (where σ is the ratio between pressure and surface pressure).

To account for thermal conduction in the icy ground, we used a 18-layers thermal diffusion soil model. Mid-layers depths range from $d_0 \sim 0.1$ mm to $d_{17} \sim 18$ m, following the power law $d_n = d_0 \times 2^n$ with n being the corresponding soil level, chosen to take into account both diurnal and seasonal thermal waves. We assumed thermal inertia of the ground ice to be constant and equal to $2000 \text{ J m}^{-2} \text{ s}^{-1/2} \text{ K}^{-1}$.

We considered (in GCM simulations) the internal heat flux and/or the thermal heat flux F_{ground} conducted from an hypothetical underlying ocean to be zero¹².

A.2 Radiative Transfer

The GCM includes a generalized radiative transfer for a variable gaseous atmospheric composition made of a mix of CO_2 , N_2 and H_2O (HITRAN 2012 database (Rothman et al., 2013)) using the correlated-k method (Fu and Liou, 1992; Eymet et al., 2016)) suited for fast calculation. For this, we decomposed atmospheric temperatures, pressures, and water vapor mixing ratio into the following respective $7 \times 8 \times 8$ grid, similar to Charnay et al. (2013): Temperatures = $\{100, 150, \dots, 350, 400\}$ K ; Pressures = $\{10^{-6}, 10^{-5}, \dots, 1, 10\}$ bars ; H_2O Mixing Ratio = $\{10^{-7}, 10^{-6}, \dots, 10^{-2}, 10^{-1}\}$ mol of H_2O / mol of air ($\text{H}_2\text{O} + \text{CO}_2$ here).

CO_2 collision-induced absorptions (CIA) and dimer absorption (Wordsworth et al., 2010)) were included in our calculations as in Forget et al. (2013) and Wordsworth et al. (2013), as well as N_2 - N_2 collision-induced absorption (Richard

¹²This is a reliable assumption for thick enough (typically > 100 m) water ice covers expected on hard Snowball Earth-like planets.

et al., 2012) and its role on the pressure broadening. We also added H₂O self and foreign continuums calculated with the CKD model (Clough et al., 1989), with H₂O lines truncated at 25 cm⁻¹.

For the computation, we used 32 spectral bands in the thermal infrared and 36 in the visible domain. 16 non-regularly spaced grid points were used for the g-space integration, where g is the cumulated distribution function of the absorption data for each band. We used a two-stream scheme (Toon et al., 1989) to take into account radiative effects of aerosols (CO₂ ice and H₂O clouds) and Rayleigh scattering (mostly by N₂ and CO₂ molecules), using the method of Hansen and Travis (1974).

We note that, for the calculation of absorption coefficients, we used only main isotopes: ¹²C¹⁶O₂ and ¹H₂¹⁶O and ¹²N₂. It has been shown in similar conditions (Halevy et al., 2009) that the radiative effect of isotopic composition should be small. Nonetheless, we take this opportunity to encourage dedicated studies about the influence of isotopic composition on the radiative properties of (thick) atmospheres.

A.3 H₂O and CO₂ physical properties

Both CO₂ and H₂O cycles are included in the GCM used in this work.

1. Melting, freezing, condensation, evaporation, sublimation and precipitation of H₂O physical processes are all included in the model. In the atmosphere, water vapor can condense into water ice particles clouds. At the surface, we fix the H₂O ice albedo at 0.6¹³ and we use an emissivity of 1.

2. In our model, CO₂ can condense to form CO₂ ice clouds and surface frost if the temperature drops below the saturation temperature. Atmospheric CO₂ ice particles are sedimented and thus can accumulate at the surface. The

¹³This is the standard value used in the Snowball Model Intercomparison (SNOWMIP) project (Pierrehumbert et al., 2011).

Physical parameters	Values
H ₂ O ice Albedo	0.6
H ₂ O ice thermal conductivity	2.5 W m ⁻¹ K ⁻¹
H ₂ O ice emissivity	1.0
Ground H ₂ O ice thermal inertia	2000 J m ⁻² s ^{-1/2} K ⁻¹
CO ₂ ice Albedo	0.6
CO ₂ ice thermal conductivity	0.5 W m ⁻¹ K ⁻¹
CO ₂ ice emissivity	0.9
CO ₂ ice density	1.5
Surface Topography	Flat
Surface roughness coefficient	0.01 m

Table 2: Physical Parameterizations used for the GCM calculations.

CO₂ ice layer formed at the surface can sublimate and recycle the CO₂ in the atmosphere. The CO₂ ice on the surface contributes to the surface albedo calculation: if the CO₂ ice layer exceeds a threshold value of 1 mm thickness, then the local surface albedo is set immediately to the albedo of CO₂ ice (0.6 in this work). On Mars, the albedo of CO₂ ice can substantially vary (Kieffer et al., 2000) with insolation and presence of dust. Without dust, the albedo can become very high so that 0.6 is probably a lower estimate. For CO₂ ice, we use an emissivity of 0.9. The radiative effect of CO₂ ice clouds is discussed in details in section 3.3

Physical parameters used for both CO₂ and H₂O ices are summarized in table 2.

B Computation of maximal CO₂ ice thickness before basal melting

Compared to water ice, the temperature dependence of CO₂ ice thermal conductivity is rather flat in the 100-250 K range (Schmitt et al. 1997; Part I, Figure 4). We can thus estimate with a good approximation the maximum CO₂ ice thickness h_{\max} (limited by basal melting) by:

$$h_{\max} = \frac{\lambda_{\text{CO}_2} (T_{\text{melt}} - T_{\text{surf}})}{F_{\text{geo}}}, \quad (7)$$

where λ_{CO_2} is the thermal conductivity of CO₂ ice, T_{surf} is the temperature at the top of the glacier and T_{melt} is the melting temperature of CO₂ ice at the base of the glacier.

We derive then T_{melt} using the Clausius-Clapeyron relation (CO₂ solid-liquid equilibrium) at the base of the glacier:

$$T_{\text{melt}} = T_{\text{ref}} e^{\frac{(\frac{1}{\rho_{\text{liq}}} - \frac{1}{\rho_{\text{sol}}})}{L_{\text{fus}}} (g\rho_{\text{sol}}h_{\max} + P_{\text{CO}_2} + P_{\text{N}_2} - P_{\text{ref}})}, \quad (8)$$

with ρ_{sol} and ρ_{liq} the volumetric mass of liquid and solid CO₂, L_{fus} the latent heat of fusion of CO₂ ice, P_{ref} and T_{ref} the coordinates of the triple point of CO₂, and P_{CO_2} and P_{N_2} the partial surface pressures of CO₂ and N₂, respectively. The pressure at the base of the glacier P_{melt} is estimated from the equation $h_{\max} = \frac{(P_{\text{melt}} - P_{\text{surf}})}{g \rho_{\text{sol}}}$, with $P_{\text{surf}} = P_{\text{CO}_2} + P_{\text{N}_2}$. We remind that we choose $p_{\text{N}_2} = 1$ bar for all our simulations.

We now derive the surface temperature T_{surf} as a function of the surface pressure P_{surf} , using another Clausius-Clapeyron relation (CO₂ solid-gas equilibrium):

$$T_{\text{surf}} = \frac{1}{\frac{1}{T_{\text{ref}}} - \frac{R}{L_{\text{sub}} M_{\text{CO}_2}} \ln\left(\frac{P_{\text{CO}_2}}{P_{\text{ref}}}\right)}, \quad (9)$$

with L_{sub} the latent heat of sublimation of CO_2 ice and M_{CO_2} the molar mass of CO_2 . It is in fact assumed here that the global mean temperature at the top of the CO_2 polar ice caps is constant and equal to the temperature of condensation of CO_2 . This approximation should remain valid as soon as there is enough CO_2 in the atmosphere (or CO_2 stays a dominant atmospheric species).

From the set of equations 7-9, we get a new equation on h_{max} of the form $h_{\text{max}} = e^{h_{\text{max}}}$, after several variable changes. We solve explicitly this equation using the lambert W function, and we obtain the following expression of the maximum possible CO_2 ice cap thickness h_{max} :

$$\left\{ \begin{array}{l} h_{\text{max}} = \frac{\lambda_{\text{CO}_2}}{F_{\text{geo}}} \left(\frac{1}{\frac{1}{T_{\text{ref}}} - \frac{R}{L_{\text{sub}} M_{\text{CO}_2}} \ln\left(\frac{P_{\text{surf}}}{P_{\text{ref}}}\right)} \right) \\ - \frac{L_{\text{fus}}}{\left(\frac{1}{\rho_{\text{liq}}} - \frac{1}{\rho_{\text{sol}}}\right) g \rho_{\text{CO}_2}} \times W \left(\frac{-\left(\frac{1}{\rho_{\text{liq}}} - \frac{1}{\rho_{\text{sol}}}\right) g \rho_{\text{CO}_2} \lambda_{\text{CO}_2} T_{\text{ref}} e^{\frac{\left(\frac{1}{\rho_{\text{liq}}} - \frac{1}{\rho_{\text{sol}}}\right)}{L_{\text{fus}}} (P_{\text{surf}} - P_{\text{ref}})}}{L_{\text{fus}} F_{\text{geo}}} \right) \\ \times e^{\frac{\left(\frac{1}{\rho_{\text{liq}}} - \frac{1}{\rho_{\text{sol}}}\right) g \rho_{\text{CO}_2} \lambda_{\text{CO}_2}}{L_{\text{fus}} F_{\text{geo}}} \left(\frac{1}{\frac{1}{T_{\text{ref}}} - \frac{R}{L_{\text{sub}} M_{\text{CO}_2}} \ln\left(\frac{P_{\text{surf}}}{P_{\text{ref}}}\right)} \right)} \end{array} \right. \quad (10)$$

This equation is used to directly compute h_{max} as a function of the internal heat flux and CO_2 partial pressure (see Figure 5).

Note that we assumed a CO_2 ice volumetric mass density of 1500 kg m^{-3} and a CO_2 ice thermal conductivity of $0.5 \text{ W m}^{-1} \text{ K}^{-1}$ (Schmitt et al. 1997; Part I, Figure 4).

C Stability of CO_2 ice caps

What happens once CO_2 ice caps have reached their maximum size, as calculated in section 4.1.4 ? Using calculations, we show in this appendix that, depending on a few parameters, the CO_2 ice caps when full may (or may not) be stable.

The total mass of CO₂ available at the surface and in the atmosphere is:

$$M_{\text{tot}} = M_{\text{atm}} + M_{\text{surf}} = \frac{SP_{\text{CO}_2}}{g} + Ah_{\text{mean}}\rho_{\text{CO}_2}, \quad (11)$$

with A the area of the CO₂ ice caps, S the total area of the surface (i.e. $4\pi R_p^2$) and h_{mean} the thickness of the CO₂ ice caps averaged over A . When CO₂ ice caps are full, $h_{\text{mean}} = h_{\text{mean}}^{\text{max}}$.

We assume now that the system – initially with full CO₂ ice caps – is slightly perturbed from $P_{\text{CO}_2} = P$ to $P + \delta P$. By conservation of CO₂ mass, the new mass of CO₂ ice caps is $M_{\text{surf}}[P + \delta P] = \rho_{\text{CO}_2} Ah_{\text{mean}}[P + \delta P]$ ¹⁴.

If this quantity is lower than the maximum mass of CO₂ ice caps, e.g. $\rho_{\text{CO}_2} Ah_{\text{mean}}^{\text{max}}[P + \delta P]$, then the system is stable. Otherwise, the condition of instability can be written formally:

$$\rho_{\text{CO}_2} Ah_{\text{mean}}[P + \delta P] > \rho_{\text{CO}_2} Ah_{\text{mean}}^{\text{max}}[P + \delta P], \quad (12)$$

which can be rewritten, using mass conservation:

$$M_{\text{tot}} - \frac{S [P + \delta P]}{g} > \rho_{\text{CO}_2} Ah_{\text{mean}}^{\text{max}}[P + \delta P], \quad (13)$$

and using Taylor series:

$$M_{\text{tot}} - \frac{S P}{g} - \frac{S \delta P}{g} > \rho_{\text{CO}_2} Ah_{\text{mean}}^{\text{max}}[P] + \delta P \rho_{\text{CO}_2} \frac{d(Ah_{\text{mean}}^{\text{max}})}{dP_{\text{CO}_2}}[P]. \quad (14)$$

Assuming that CO₂ ice caps were initially full, this yields to $h_{\text{mean}}[P] = h_{\text{mean}}^{\text{max}}[P]$

¹⁴Hereafter, '[' and ']' are used to bracket variables.

and gives:

$$\left(M_{\text{tot}} - \frac{S P}{g} - \rho_{\text{CO}_2} A h_{\text{mean}}[P]\right) - \frac{S \delta P}{g} > \delta P \rho_{\text{CO}_2} \frac{d(A h_{\text{mean}}^{\text{max}})}{dP_{\text{CO}_2}}[P]. \quad (15)$$

For $\delta P > 0$, we have then:

$$A \frac{dh_{\text{mean}}^{\text{max}}}{dP_{\text{CO}_2}}[P] + h_{\text{mean}}^{\text{max}} \frac{dA}{dP_{\text{CO}_2}}[P] < -\frac{S}{\rho_{\text{CO}_2} g}. \quad (16)$$

We know first from GCM simulations that the area of the ice caps A is not a monotonic function of P_{CO_2} (see Figure 2). A is in fact extremely rich in information, because it depends on a subtle combination of the greenhouse effect of CO_2 , the surface thermal emission, the condensation temperature of CO_2 and the global heat atmospheric redistribution. As P_{CO_2} grows, GCM simulations tell us that $\frac{dA}{dP_{\text{CO}_2}}$ should vary from positive to negative values. Fortunately, we also know from the various GCM simulations shown in Figure 2b (23.5° obliquity, radiatively inactive CO_2 clouds) that the maximum of $A(P_{\text{CO}_2})$ should for example roughly lie at a CO_2 partial pressure of 1 bar in this specific configuration.

It is possible to derive an analytical - complicated yet - expression of $\frac{dh_{\text{mean}}^{\text{max}}}{dP_{\text{CO}_2}}$ using equations 10 and 4. It tells us that, whatever the configuration, $\frac{dh_{\text{mean}}^{\text{max}}}{dP_{\text{CO}_2}}$ is always negative. As p_{CO_2} increases, the temperature at the top of the CO_2 ice caps also increases, which limits the thickness of the CO_2 ice caps¹⁵ (see equation 1).

We illustrate now the previous calculations with the experiment extensively described in this work (1.30 AU, 23.5° obliquity, radiatively inactive CO_2 ice clouds, CO_2 partial pressure of 1 bar). Based on GCM simulations, we assume

¹⁵Equation 4 shows that the mean thickness of the CO_2 ice caps is proportional to the maximum thickness calculated by basal melting.

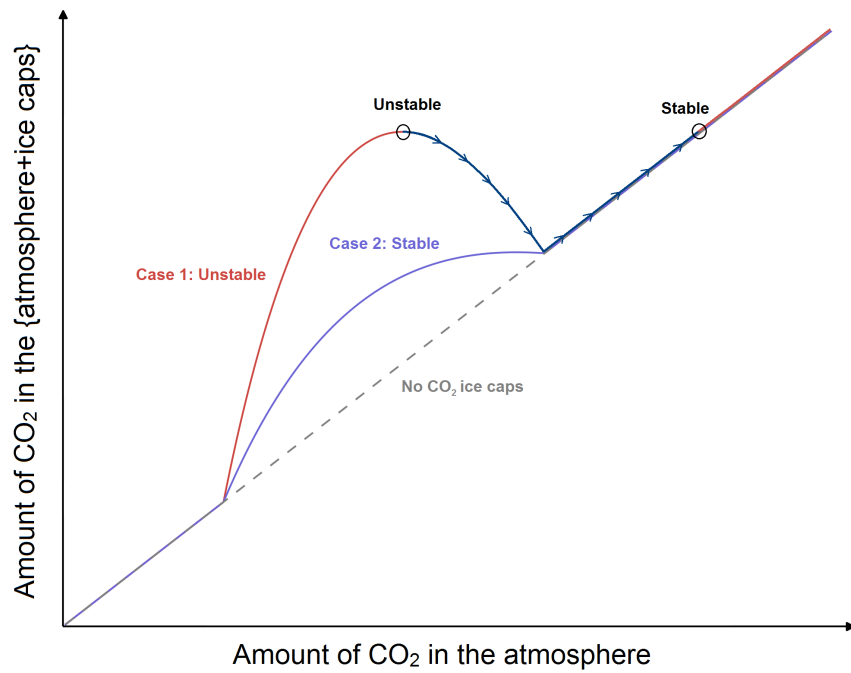


Figure 7: Qualitative estimates of the maximum amount of CO₂ in the {surface, atmosphere} as a function of the CO₂ partial pressure, for two different scenarios. In the first scenario (case 1), the CO₂ ice caps when full would be unstable. All the CO₂ ice get sublimed, forming a dense CO₂ atmosphere. In the second scenario (case 2), the CO₂ ice caps when full should progressively shrink as the CO₂ partial pressure increases, but would not be unstable. This configuration occurs when the decrease of the size of the CO₂ ice caps is offset by the increase of the CO₂ atmospheric mass.

that $\frac{dA}{dP_{\text{CO}_2}}|_{p\text{CO}_2=1\text{bar}} \sim 0 \text{ m}^2 \text{ Pa}^{-1}$ and we have therefore (with $\frac{A}{S} \sim 0.1$; see section 4.1.1):

$$\frac{dh_{\text{mean}}^{\text{max}}}{dP_{\text{CO}_2}} < -\frac{S}{gA\rho_{\text{CO}_2}} = \frac{-10}{9.81 \times 1.5 \times 10^3} = -7 \times 10^{-4} \text{ m Pa}^{-1}. \quad (17)$$

Our calculations indicate that this condition is valid for an internal heat flux roughly lower than 80 mW m^{-2} (case 1 in Figure 7). It means that, for an internal heat flux lower than 80 mW m^{-2} : (1) CO_2 ice caps when full would not be stable, and (2) the maximum amount of CO_2 that can be trapped in the {surface, atmosphere} system is attained for $p\text{CO}_2$ lower or equal to 1 bar.

Conversely, for an internal heat flux higher than 80 mW m^{-2} (case 2 in Figure 7), CO_2 ice caps when full would be stable (unless $\frac{dA}{dP_{\text{CO}_2}}$ term becomes somehow significant).

References

- Abbot, D. S. and Pierrehumbert, R. T. (2010). Mudball: Surface dust and Snowball Earth deglaciation. *Journal of Geophysical Research (Atmospheres)*, 115:3104A.
- Abbot, D. S. (2016). Analytical Investigation of the Decrease in the Size of the Habitable Zone Due to a Limited CO_2 Outgassing Rate. *The Astrophysical Journal*, 827:117.
- Brantley, S. L. and Koepenick, K. W. (1995). Measured carbon dioxide emissions from Oldoinyo Lengai and the skewed distribution of passive volcanic fluxes. *Geology*, 23:933.
- Charnay, B., Forget, F., Wordsworth, R., Leconte, J., Millour, E., Codron, F., and Spiga, A. (2013). Exploring the faint young sun problem and the possible

- climates of the archean earth with a 3-d gcm. *Journal of Geophysical Research : Atmospheres*, 118:414–431.
- Clough, S., Kneizys, F., and Davies, R. (1989). Line shape and the water vapor continuum. *Atmospheric Research*.
- Cuffey, K. and Paterson, W. (2010). *The physics of glaciers*. Academic Press.
- Davies, J. H. (2013). Global map of solid Earth surface heat flow. *Geochemistry, Geophysics, Geosystems*, 14:4608–4622.
- Durham, W. B., Kirby, S. H., and Stern, L. A. (1999). Steady-state flow of solid CO₂: Preliminary results. *Geophysical Research Letter*, 26:3493–3496.
- Durham, W. B. and Stern, L. A. (2001). Rheological Properties of Water Ice—Applications to Satellites of the Outer Planets. *Annual Review of Earth and Planetary Sciences*, 29:295–330.
- Durham, W. B., Stern, L. A., and Kirby, S. H. (2001). Rheology of ice I at low stress and elevated confining pressure. *Journal of Geophysical Research*, 106:11031–11042.
- Evans, D. A., Beukes, N. J., and Kirschvink, J. L. (1997). Low-latitude glaciation in the palaeoproterozoic era. *Nature*, 386:262.
- Eymet, V., Coustet, C., and Piaud, B. (2016). kspectrum: an open-source code for high-resolution molecular absorption spectra production. In *Journal of Physics Conference Series*, volume 676 of *Journal of Physics Conference Series*, page 012005.
- Forget, F. and Pierrehumbert, R. T. (1997). Warming early Mars with carbon dioxide clouds that scatter infrared radiation. *Science*, 278:1273–1276.

- Forget, F., Wordsworth, R., Millour, E., Madeleine, J.-B., Kerber, L., Leconte, J., Marcq, E., and Haberle, R. M. (2013). 3D modelling of the early martian climate under a denser CO₂ atmosphere: Temperatures and CO₂ ice clouds. *Icarus*, 222:81–99.
- Fowler, A. (2011). *Mathematical Geoscience*. Springer.
- Fu, Q. and Liou, K. N. (1992). On the correlated k-distribution method for radiative transfer in nonhomogeneous atmospheres. *Journal of the Atmospheric Sciences*, 49.
- Goldsby, D. L. and Kohlstedt, D. L. (2001). Superplastic deformation of ice: Experimental observations. *Journal of Geophysical Research*, 106:11.
- Gough, D. O. (1981). Solar interior structure and luminosity variations. *Solar Phys.*, 74:21–34.
- Halevy, I., Pierrehumbert, R. T., and Schrag, D. P. (2009). Radiative transfer in CO₂-rich paleoatmospheres. *Journal of Geophysical Research (Atmospheres)*, 114.
- Hansen, J. E. and Travis, L. D. (1974). Light scattering in planetary atmosphere. *Space Sci. Rev.*, 16:527–610.
- Haqq-Misra, J., Kopparapu, R. K., Batalha, N. E., Harman, C. E., and Kasting, J. F. (2016). Limit Cycles Can Reduce the Width of the Habitable Zone. *The Astrophysical Journal*, 827:120.
- Hoffman, P. F., Kaufman, A. J., Halverson, G. P., and Schrag, D. P. (1998). A neoproterozoic snowball Earth. *Science*, 281:1342–1346.
- Hoffman, P. F. and Schrag, D. P. (2002). The snowball earth hypothesis : Testing the limits of global change. *Terra Nova*, 14:129–155.

- Hourdin, F., Musat, I., Bony, S., Braconnot, P., Codron, F., Dufresne, J.-L., Fairhead, L., Filiberti, M.-A., Friedlingstein, P., Grandpeix, J.-Y., Krinner, G., Levan, P., Li, Z.-X., and Lott, F. (2006). The LMDZ4 general circulation model: climate performance and sensitivity to parametrized physics with emphasis on tropical convection. *Climate Dynamics*, 27:787–813.
- Jarrard, R. D. (2003). Subduction fluxes of water, carbon dioxide, chlorine, and potassium. *Geochemistry, Geophysics, Geosystems*, 4.
- Joshi, M. M. and Haberle, R. M. (2012). Suppression of the Water Ice and Snow Albedo Feedback on Planets Orbiting Red Dwarf Stars and the Subsequent Widening of the Habitable Zone. *Astrobiology*, 12:3–8.
- Kaspi, Y. and Showman, A. P. (2015). Atmospheric Dynamics of Terrestrial Exoplanets over a Wide Range of Orbital and Atmospheric Parameters. *The Astrophysical Journal*, 804:60.
- Kasting, J., Whitmire, D. P., and Reynolds, R. T. (1993). Habitable zones around main sequence stars. *Icarus*, 101:108–128.
- Kieffer, H. H., Titus, T. N., Mullins, K. F., and Christensen, P. R. (2000). Mars south polar spring and summer behavior observed by TES: Seasonal cap evolution controlled by frost grain size. *Journal of Geophysical Research*, 105:9653–9700.
- Kitzmann, D. (2016). Revisiting the Scattering Greenhouse Effect of CO₂ Ice Clouds. *The Astrophysical Journal Letters*, 817.
- Kopparapu, R. K., Ramirez, R., Kasting, J. F., Eymet, V., Robinson, T. D., Mahadevan, S., Terrien, R. C., Domagal-Goldman, S., Meadows, V., and Deshpande, R. (2013). Habitable Zones around Main-sequence Stars: New Estimates. 765:131.

- Kopparapu, R. K., Ramirez, R. M., SchottelKotte, J., Kasting, J. F., Domagal-Goldman, S., and Eymet, V. (2014). Habitable Zones around Main-sequence Stars: Dependence on Planetary Mass. *The Astrophysical Journal Letters*, 787.
- Krawczynski, M. J., Behn, M. D., Das, S. B., and Joughin, I. (2009). Constraints on the lake volume required for hydro-fracture through ice sheets. *Geophysical Research Letters*, 36:L10501.
- Kump, L. R., Brantley, S. L., and Arthur, M. A. (2000). Chemical weathering, atmospheric co₂ and climate. *Annu. Rev. Earth Planet. Sci.*, 28:611.
- Lide, D. (2004). *CRC Handbook of Chemistry and Physics: A Ready-reference Book of Chemical and Physical Data 85th ed.* CRC Press.
- Paterson, D. (2010). *The Physics of Glaciers* Academic Press.
- Longhi, J. (2005). Phase equilibria in the system CO₂-H₂O I: New equilibrium relations at low temperatures. *Geochimica et Cosmochimica Acta*, 69:529–539.
- Menou, K. (2013). Water-trapped Worlds. *The Astrophysical Journal*, 774.
- Menou, K. (2015). Climate stability of habitable Earth-like planets. *Earth and Planetary Science Letters*, 429:20–24.
- Nye, J. F., Durham, W. B., Schenk, P. M., and Moore, J. M. (2000). The Instability of a South Polar Cap on Mars Composed of Carbon Dioxide. *Icarus*, 144:449–455.
- Pierrehumbert, R. T. (2005). Climate dynamics of a hard snowball Earth. *Journal of Geophysical Research (Atmospheres)*, 110.
- Pierrehumbert, R. T., Abbot, D. S., Voigt, A., and Koll, D. (2011). Climate of

- the Neoproterozoic. *Annual Review of Earth and Planetary Sciences*, 39:417–460.
- Richard, C., Gordon, I. E., Rothman, L. S., Abel, M., Frommhold, L., Gustafsson, M., Hartmann, J.-M., Hermans, C., Lafferty, W. J., Orton, G. S., Smith, K. M., and Tran, H. (2012). New section of the HITRAN database: Collision-induced absorption (CIA). *Journal of Quantitative Spectroscopy and Radiative Transfer*, 113:1276–1285.
- Rothman, L. S., Gordon, I. E., Babikov, Y., Barbe, A., Benner, D. C., Bernath, P. F., Birk, M., Bizzocchi, L., Boudon, V., Brown, L. R., Campargue, A., Chance, K., Coudert, L. H., Devi, V. M., Drouin, B. J., Fayt, A., Flaud, J.-M., Gamache, R. R., Harrison, J. J., Hartmann, J. M., Hill, C., Hodges, J. T., Jacquemart, D., Jolly, A., Lamouroux, J., Le Roi, R. J., Li, G., Long, D. A., Lyulin, O. M., Mackie, C. J., Massie, S. T., Mikhailenko, S., Miller, H. S. P., Naumenko, O. V., Nikitin, A. V., Orphal, J., Perevalov, V. I., Perrin, A., Polovtseva, E. R., Richard, C., Smith, M. A. H., Starikova, E., Sung, K., Tashkun, S. A., Tennyson, J., Toon, G. C., Tyuterev, V. G., and Wagner, G. (2013). The HITRAN2012 molecular spectroscopic database. *J. Quant. Spectrosc. Radiat. Transfer*, 130:4–55.
- Schmitt, B., De Bergh, C., and Festou, M. (1997). *Solar System Ices*. Kluwer Academic.
- Seager S., Kuchner M., Hier-Majumder C. A. and Militzer, B. (2007). Mass-Radius Relationships for Solid Exoplanets. *The Astrophysical Journal Letters*, 669:1279-1297.
- Sloan, E. (1998). *Clathrate hydrates of natural gases, 2nd ed.* CRC Press.
- Span, R. and Wagner, W. (1996). A New Equation of State for Carbon Dioxide Covering the Fluid Region from the Triple-Point Temperature to 1100 K at

- Pressures up to 800 MPa. *Journal of Physical and Chemical Reference Data*, 25:1509–1596.
- Toon, O. B., McKay, C. P., Ackerman, T. P., and Santhanam, K. (1989). Rapid calculation of radiative heating rates and photodissociation rates in inhomogeneous multiple scattering atmospheres. *J. Geophys. Res.*, 94:16,287–16,301.
- Turbet, M., Leconte, J., Selsis, F., Bolmont, E., Forget, F., Ribas, I., Raymond, S. N., and Anglada-Escudé, G. (2016). The habitability of Proxima Centauri b II. Possible climates and Observability. *Astronomy & Astrophysics*, 596:A112.
- Turbet, M., Forget, F., Head, J., and Wordsworth, R. (2017). 3D Modelling of the climatic impact of outflow channel events on Early Mars. *Icarus*, 288:10-36.
- Turbet, M., Bolmont, E., Leconte, J., Forget, F., Selsis, F., Tobie, G., Caldas, A., Naar, J., and Gillon, M. (2017). Climate diversity on cool planets around cool stars with a versatile 3-D Global Climate Model: the case of TRAPPIST-1 planets. submitted to *Astronomy & Astrophysics*, [arXiv:1707.06927].
- Turcotte, D. L. and Schubert, G. (2001). *Geodynamics, 2nd ed.* Cambridge Univ. Press.
- Walker, J. C. G., Hays, P. B., and Kasting, J. F. (1981). A negative feedback mechanism for the long term stabilization of the earth’s surface temperature. *J. Geophys. Res.*, 86:9776–9782.
- Walker, J. C. G. (1985). Carbon dioxide on the early earth. *Origins of Life*, 16:117-127.
- Walker, J. C. G. and Zahnle, K. J. (1986). Lunar nodal tide and distance to the moon during the Precambrian. *Nature*, 320:600–602.

- Wordsworth, R., Forget, F., and Eymet, V. (2010). Infrared collision-induced and far-line absorption in dense CO₂ atmospheres. *Icarus*, 210:992–997.
- Wordsworth, R., Forget, F., Millour, E., Head, J. W., Madeleine, J.-B., and Charnay, B. (2013). Global modelling of the early martian climate under a denser CO₂ atmosphere: Water cycle and ice evolution. *Icarus*, 222:1–19.
- Wordsworth, R. D., Forget, F., Selsis, F., Millour, E., Charnay, B., and Madeleine, J.-B. (2011). Gliese 581d is the First Discovered Terrestrial-mass Exoplanet in the Habitable Zone. *The Astrophysical Journal Letters*, 733:L48.
- Zahnle, K. and Walker, J. C. G. (1987). A constant daylength during the precambrian era? *Precambrian Research*, 37:95–105.
- Ziethé, R. and Spohn, T. (2007). Two-dimensional stokes flow around a heated cylinder: A possible application for diapirs in the mantle. *Journal of Geophysical Research (Solid Earth)*, 112:B09403.